Supplementary Information for "Arrested maturation of excitatory synapses in autosomal dominant lateral temporal lobe epilepsy"

Yu-Dong Zhou, Sanghoon Lee, Zhe Jin, Moriah Wright, Stephen E. P. Smith, & Matthew P. Anderson

Contents

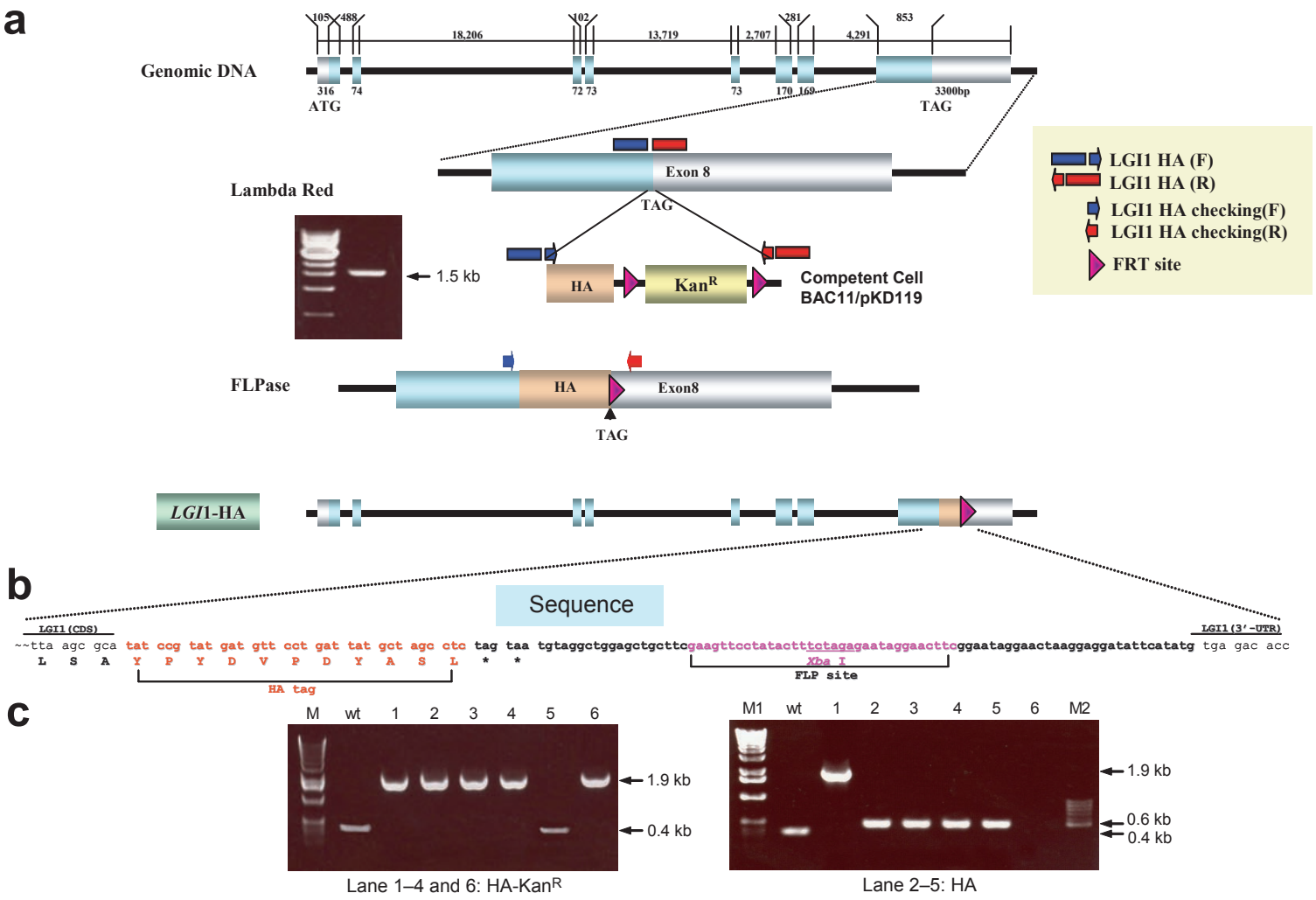

Supplementary Figure 1 Recombineering an HA tag label into the wild-type LGI1 gene (226 kb, BAC vector). (**a**) DNA sequences encoding an HA epitope tag are inserted in frame with the C-terminus of LGI1 using lamda red recombinase in E. coli. PCR generated 1.5 kb DNA fragment used for homologous recombination is shown (left). Checking primers flank the homologous arms. The FRT sequence flanked kanamycin selection cassette is removed by transfecting a plasmid encoding FLP recominase in E. coli. (**b**) The DNA sequence of the final construct identifies the HA tag in frame with LGI1 C-terminus followed by two translational stop codons. The FLP site is also present. (**c**) PCR identifies bacterial clones containing the HA-Kan cassette (lanes 1–4, 6, left). Deletion of the Kan cassette decreases the molecular weight of the PCR product to 0.6 kb. A 0.4 kb PCR product is generated by the native LGI1 gene.

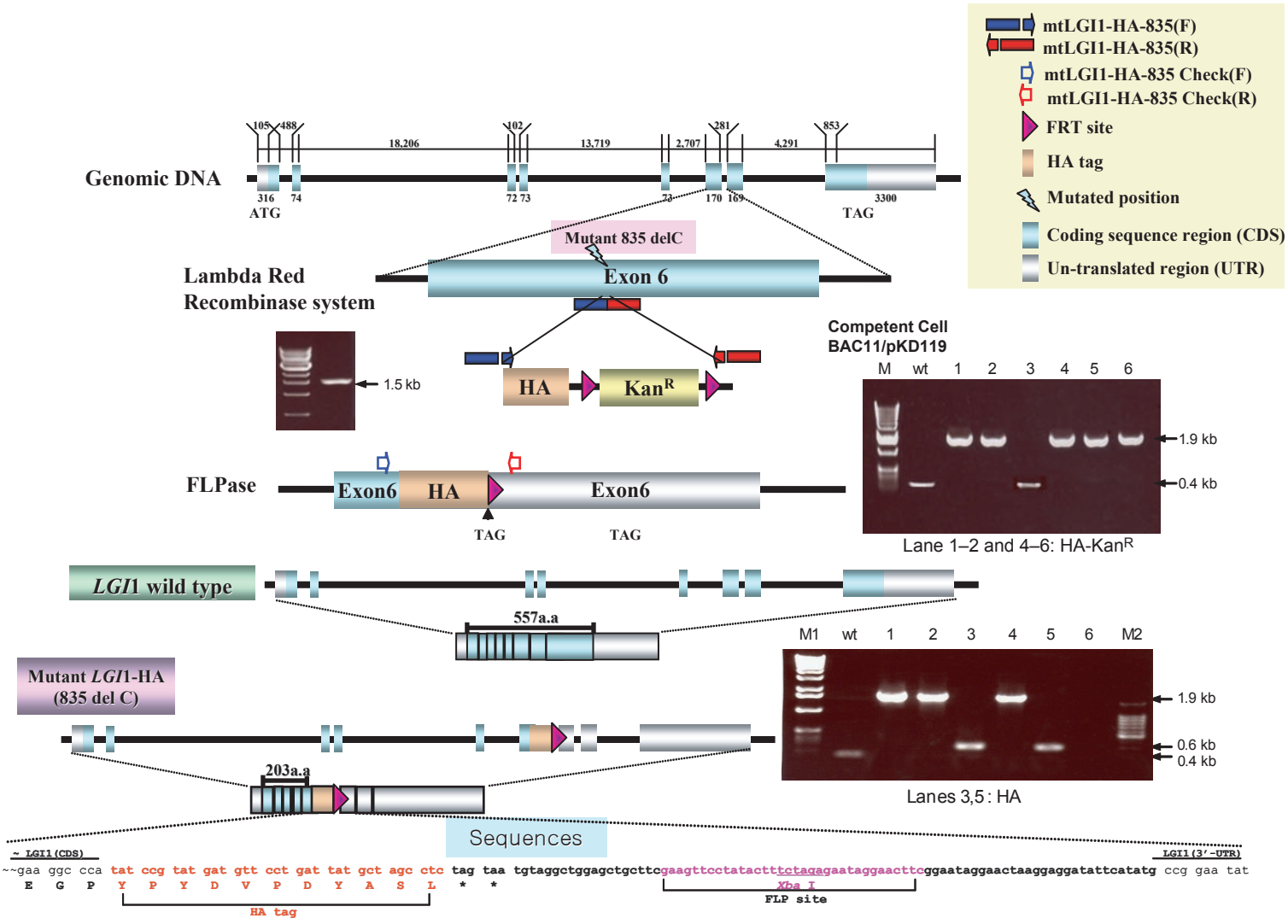

Supplementary Figure 2 Recombineering the ADLTE epilepsy mutant LGI1 gene (835delC). DNA sequences encoding an HA epitope tag are inserted in frame within exon 6 of LGI1 at amino acid 835 using lamda red recombinase in E. coli. PCR generated 1.5 kb DNA fragment used for homologous recombination is shown in the left gel. Checking primers flank the homologous arms. The FRT sequence flanked kanamycin selection cassette is removed by transfecting a plasmid encoding FLP recominase in E. coli. The DNA sequence of the final construct identifies the HA tag in frame with LGI1 followed by two translational stop codons. The FLP site is also present. Ethidium-stained agarose gel containing DNA PCR products to identify bacterial clones containing the HA-Kan cassette (lanes 1–2, 4–6, top gel). Deletion of the Kan cassette decreases the molecular weight of the PCR product to 0.6 kb (lanes 3 and 5). A 0.4 kb PCR product is generated by the native LGI1 gene.

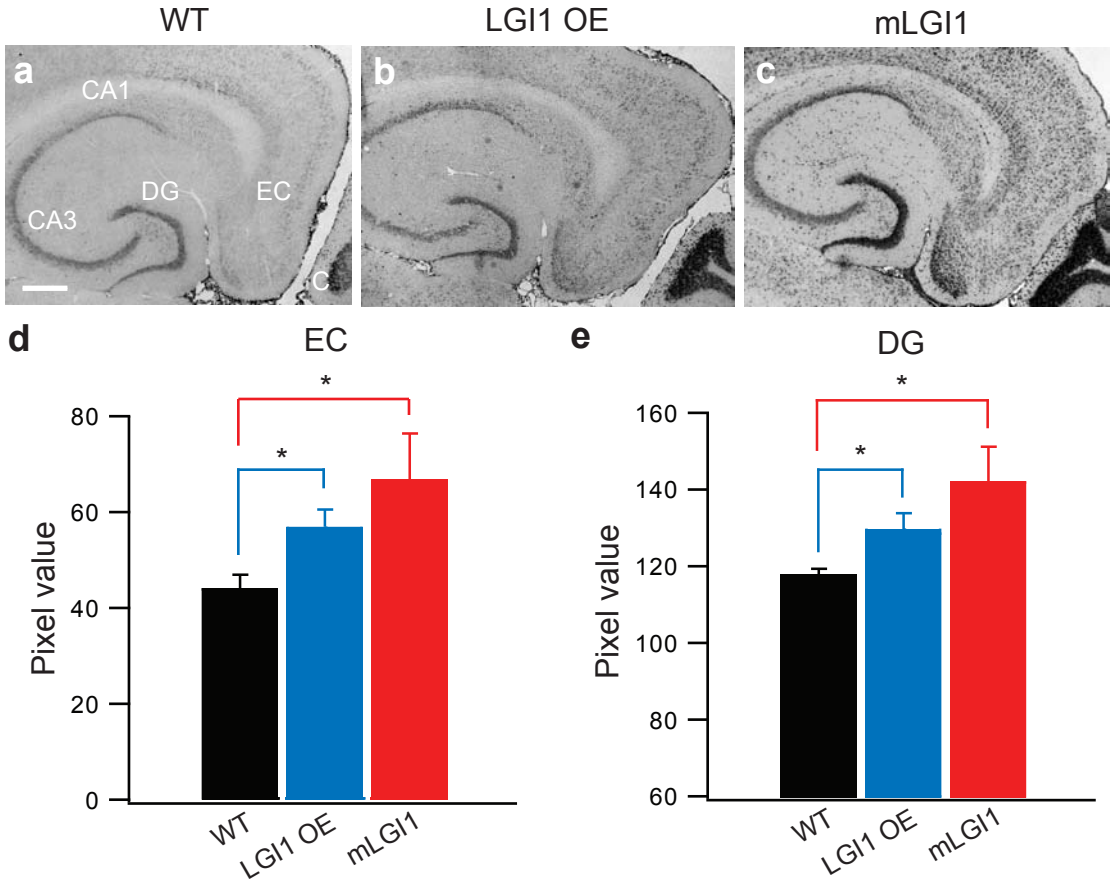

Supplementary Figure 3 LGI1 mRNA is increased in LGI1 transgenic mice. (**a–c**) *In-situ* hybridization of transverse brain sections made from wild-type (WT, **a**), full-length LGI1 carrying (LGI1 OE, **b**), and ADLTE mutant LGI1 carrying (mLGI1, **c**) mice, probed with a digoxigenin-labeled probe against LGI1 exon 1–2 junction. (**d**,**e**) Optical density of dentate gyrus (**d**) and entorhinal cortex (**e**) in WT, LGI1 OE, and mLGI1 mice. Y axis indicates arbitrary pixel values corrected for uneven backgrounds. n = 8 - 10. C, cerebellum; DG, dentate gyrus; EC, entorhinal cortex. *, $P < 0.05$. Scale bar, 500 μm.

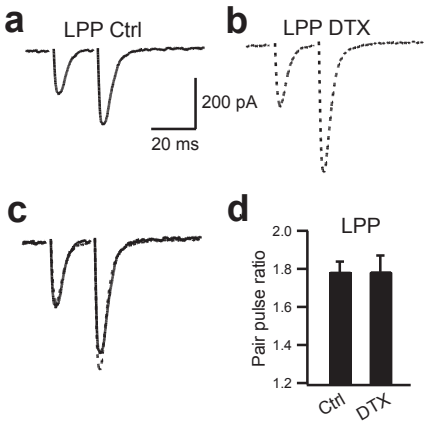

Supplementary Figure 4 α-dendrotoxin (DTX) has no effect on paired-pulse facilitation (PPF) at lateral perforant path-dentate granule cell (LPP-GC) synapse. (**a,b**) Representative traces of PPF recorded from mature GC with (dotted) (**b**) or without (Ctrl) (**a**) 100 nM DTX. (**c**) Scaling of the trace in (**a**) to the trace in (**b**). (**d**) Bar graph of paired-pulse ratio (ppr). Ctrl, *n* = 5; DTX, *n* = 5.

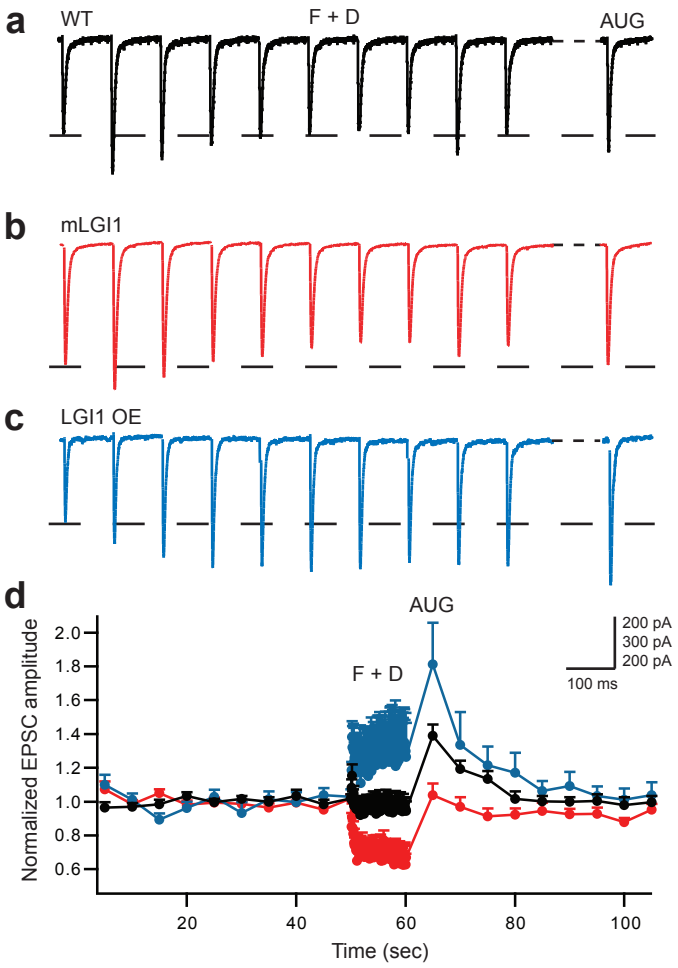

Supplementary Figure 5 LGI1 regulates short-term plasticity (STP) at MPP-GC synapses. Facilitation (F), depression (D), and augmentation (AUG) were compared. (**a–c**) 10 Hz 10 sec train stimulation reveals different forms of STP depending on the mouse genotype. In wild-type (WT) mice, the glutamatergic synapses showed neither facilitation nor depression with repeated stimulation and moderate augmentation (**a**). In mice carrying the truncated mutant form of LGI1 (mLGI1), synapses showed depression and no augmentation (**b**). In mice over-expressing full-length LGI1 (LGI1 OE), repeated stimulation caused persistent facilitation and a larger augmentation (**c**). (**d**) Time course of normalized EPSCs in WT (black symbol, *n* = 13), mLGI1 (red symbol, *n* = 13), and LGI1 OE (blue symbol, *n* = 7) mice.

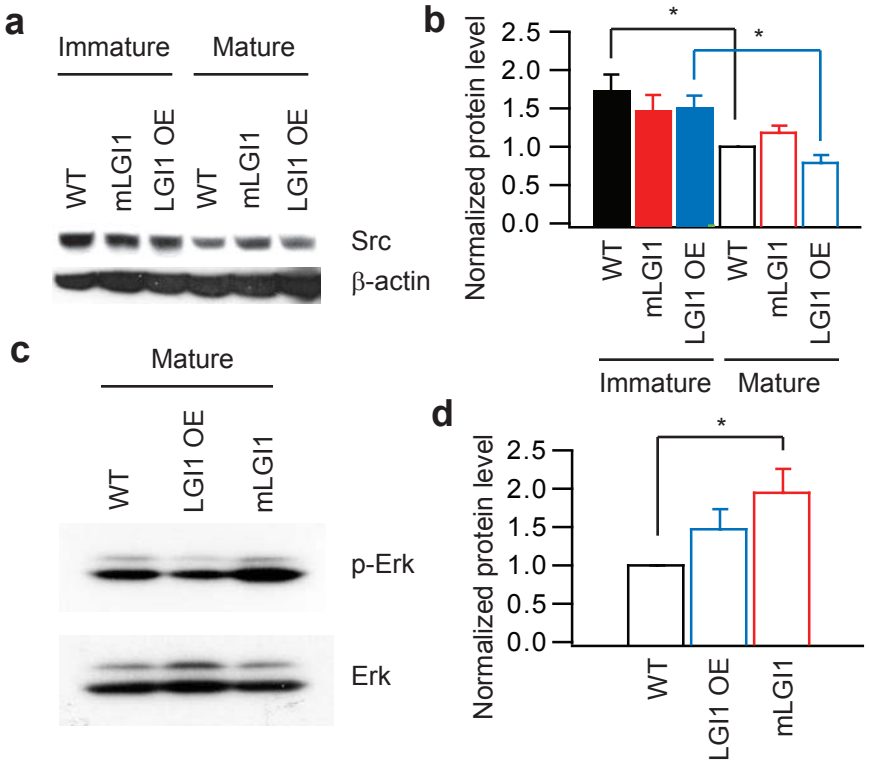

Supplementary Figure 6 Src kinase and phospho-Erk (p-Erk) are increased in ATLDE mutant LGI1 mice. (**a**) Immunoblot of Src in immature and mature wild-type (wt), mutant LGI1 (mLGI1), and LGI1 over-expressing (LGI1 OE) mice. Note a relative high level of Src in mature mLGI1 mice compared to mature wt and LGI1 OE mice. (**b**) Src expression level is significantly decreased during postnatal development in both wt and LGI1 OE mice ($P < 0.05$, $n = 6$), but not in mLGI1 mice ($P = 0.21$, $n = 6$). (**c**) Immunoblot of Erk and p-Erk in mature wt, mLGI1, and LGI1 OE mice. (**d**) p-Erk is greatly increased in mature mLGI1 mice ($P < 0.05$, $n = 7$).

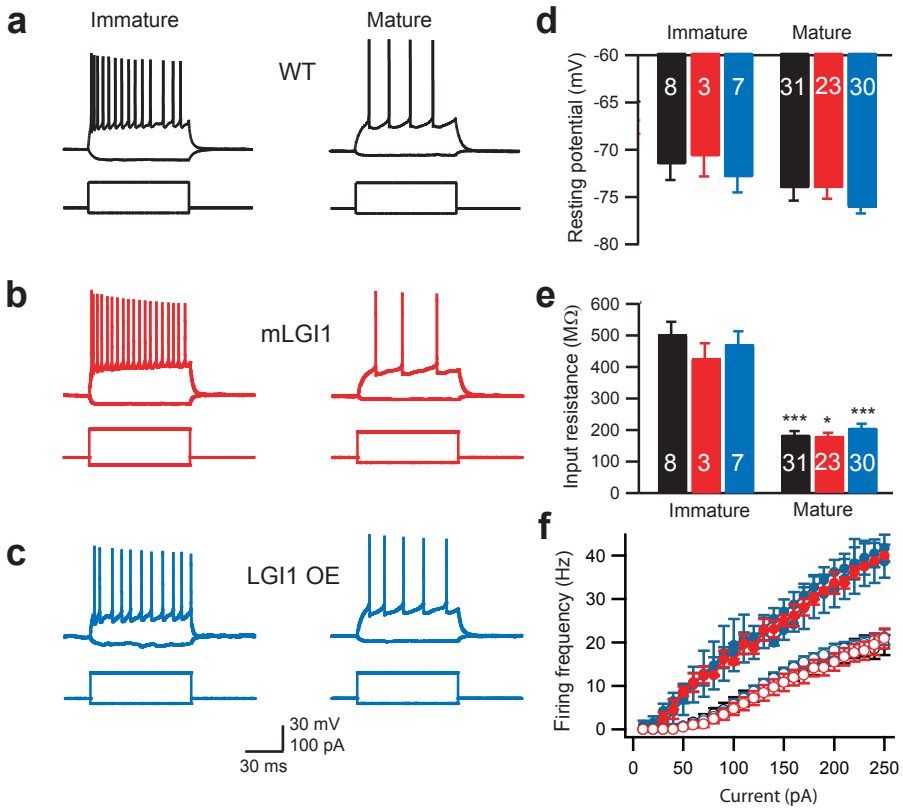

Supplementary Figure 7 Biophysical properties of the dentate granule cells (GCs) develop normally in mice over-expressing full-length LGI1 (LGI1 OE) and truncated mutant LGI1 (mLGI1) proteins compared to wild-type (WT) animals. (**a–c**) Firing behavior of immature (from p13 – p19 mice) and mature (from 1–5 month old mice) GCs in WT (**a**), mLGI1 (**b**), and LGI1 OE mice (**c**). Note a fast firing frequency in response to the depolarizing current injection in immature GCs. (**d,e**) Histogram of developmental change in GC resting potentials (**d**) and GC input resistance (**e**). Input resistance significantly decreased in mature GCs, but no significant differences across genotypes were observed. There is no significant change in resting potential at each stage of postnatal maturation, and no significant genotype differences were present. (**f**) Firing frequency plot exhibited no differences in intrinsic excitability across genotypes in immature (filled circles) ($F_{2,240}$ = 2.32, p > 0.05) and mature (open circles) ($F_{2,1139}$ = 3.12, P > 0.05 for all group comparisons) animals. *, P < 0.05; ***, P < 0.001.

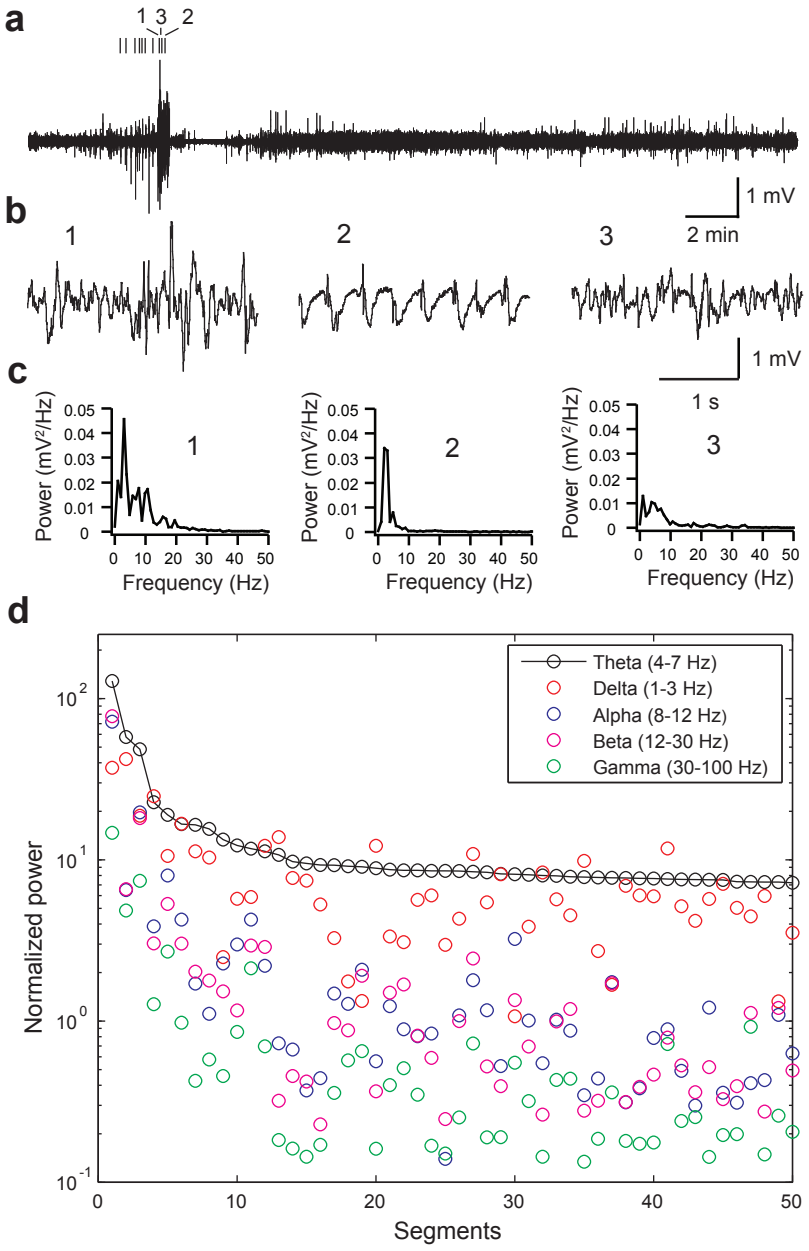

Supplementary Figure 8 Unbiased extraction of aberrant EEG segments based on theta band power. (**a**) A representative EEG trace. The positions of 10 extracted segments with highest theta band power are shown above the trace. (**b**) Expanded segments (1–3: the first three segments with highest theta band power) from (**a**). (**c**) The power spectral density (PSD) for the first three segments shown in (**b**). (**d**) Normalized PSDs of 50 most significant segments in 5 typical EEG frequency bands. Band PSDs were normalized to the background theta band PSD.

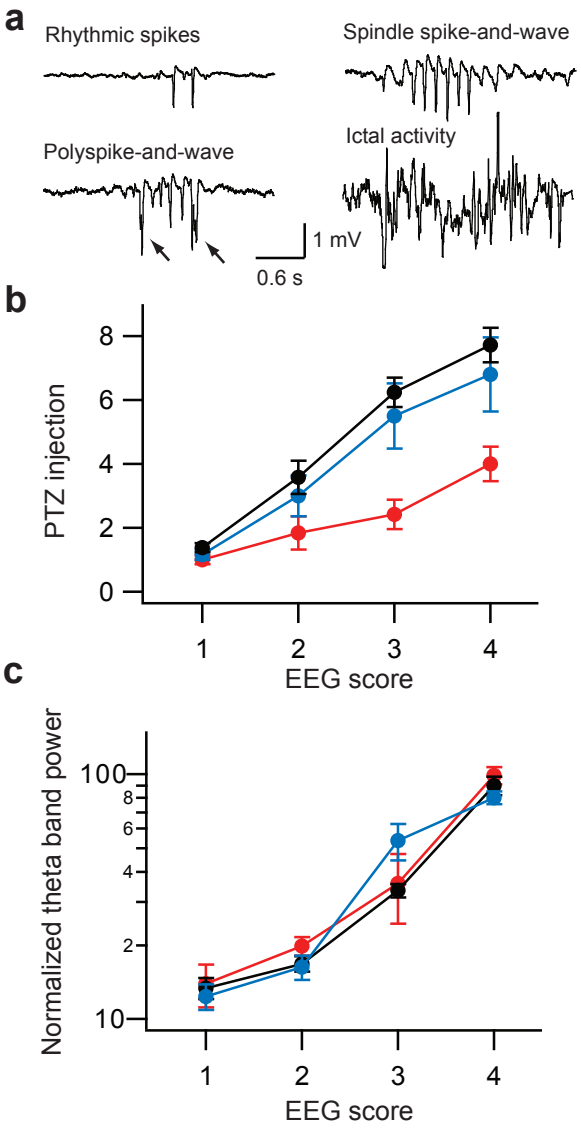

Supplementary Figure 9 Increasing normalized theta band power is associated with severity of kindling seizures. (**a**) Extracted EEG patterns associated with PTZ kindling. Rhythmic spikes, spike-and-waves, and polyspike-and-waves (arrows show polyspikes) are less severe forms of aberrant EEG patterns associated with PTZ kindling. Fully kindled animals displayed typical ictal activity comprised of decrescendo spike-and-waves. EEG score is based on the severest EEG pattern extracted from individual EEG recordings: 1, rhythmic spikes; 2, spike-and-wave; 3, polyspike-and-wave; 4, ictal activity. (**b**) The aberrant EEG patterns occurred sequentially during PTZ kindling experiments. mLGI1 mice (red, n = 8) had earlier sequential patterns than wild-type (black, n = 15) and LGI1 OE (blue, n = 7) mice ($F_{2,84}$ = 14.11, P << 0.05; mLGI1 vs wild-type, P << 0.01; mLGI1 vs LGI1 OE, P < 0.01). (**c**) Normalized theta band power increases with EEG score reflecting increasingly severe kindling. Wild-type (black), mLGI1 (red), and LGI1 OE (blue) mice showed the same trend ($F_{2,322}$ = 0.06, P = 0.94).

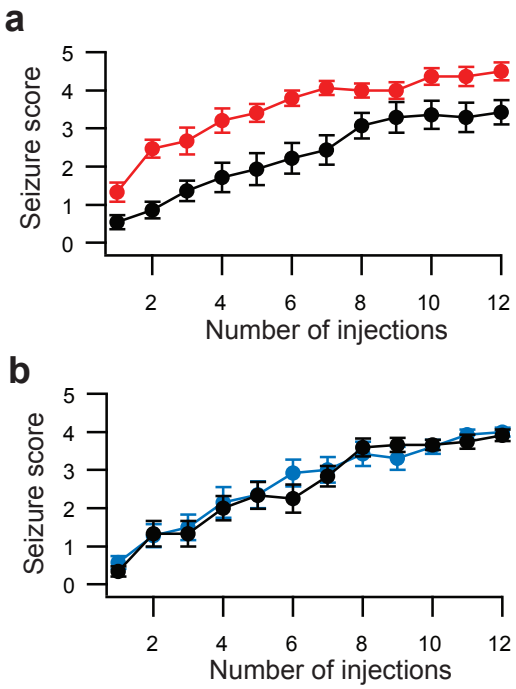

Supplementary Figure 10 ADLTE mutant LGI1 facilitates kindling epileptogenesis. (**a,b**) Behavioral seizure scores of PTZ-kindling in mLGI1 mice (red) (*n* = 15) vs their wild-type littermates (black) (*n* = 15) (**a**), and LGI1 OE mice (blue) (*n* = 14) vs their wild-type littermates (black) (*n* = 12) (**b**). 2-way ANOVA and Tukey's HSD test revealed a significant difference between mLGI1 mice and their wild-type littermates ($F_{3,604}$ = 40.58, mLGI1 vs wild-type: $P << 0.05$).

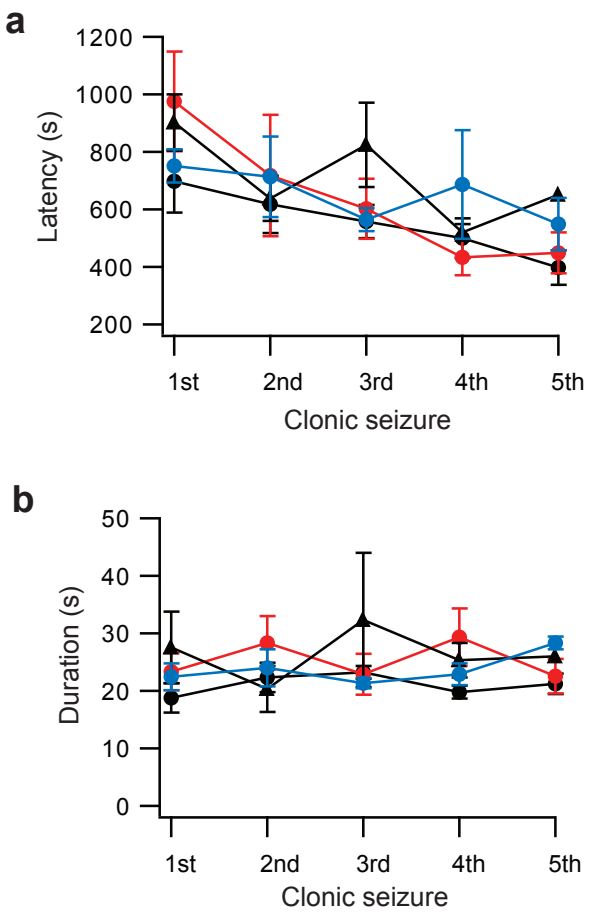

Supplementary Figure 11 Clonic seizure properties showed no differences across genotypes. There were no differences in clonic seizure latency (**a)** ($F_{3,78}$ = 0.9, P = 0.45) or duration (**b**) ($F_{3,81}$ = 1.22, P = 0.3) in kindled mLGI1 (red circles, n = 7), LGI1 OE (blue circles, n = 6), and their wild-type littermates (mLGI1 littermates: black circles, n = 6; LGI1 OE littermates: black triangles, n = 5). Note kindled mice exhibited a decrease in clonic seizure latency with further PTZ injections (**a**) while maintained a relatively constant seizure duration (**b**).

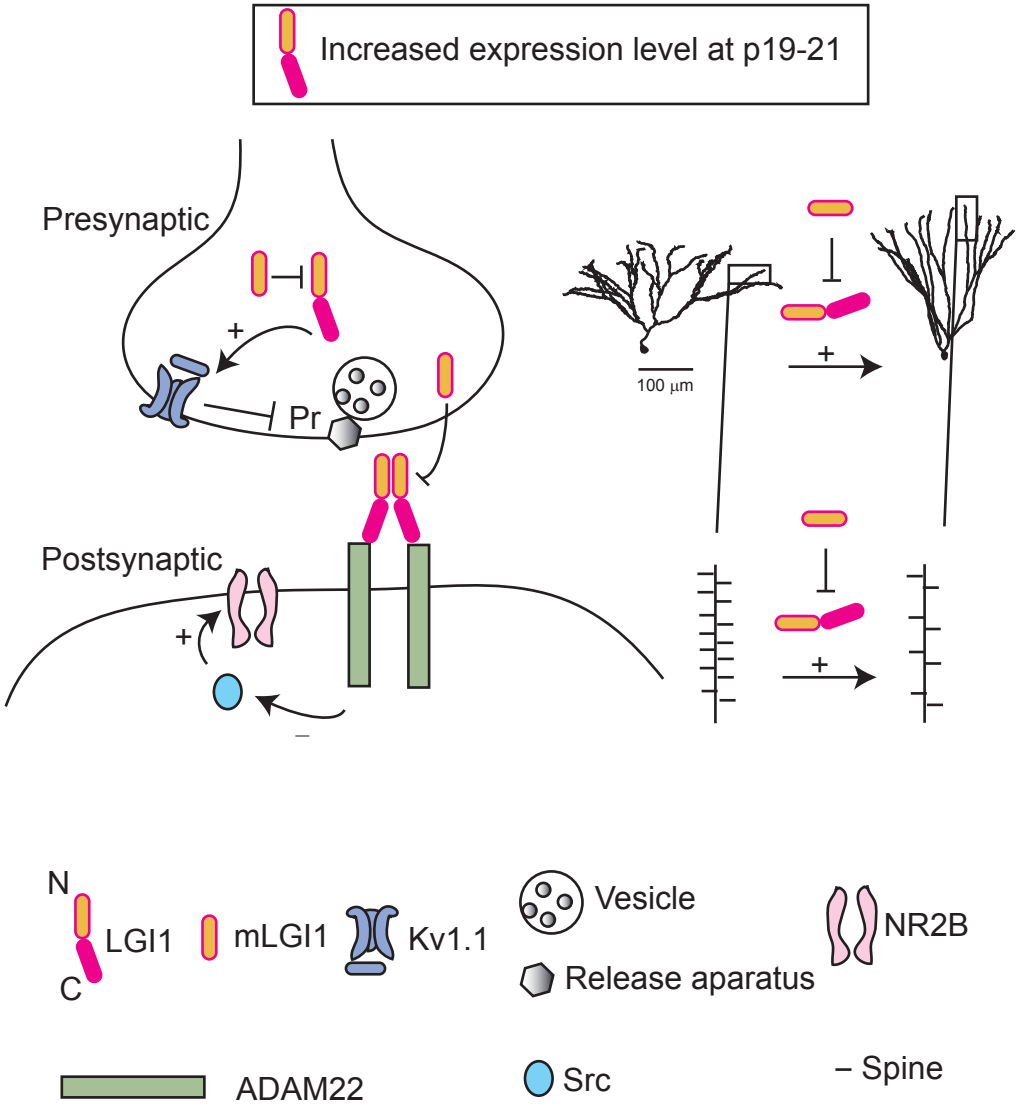

Supplementary Figure 12 LGI1 coordinates glutamatergic synapse maturation and dendritic pruning during postnatal development. LGI1 decreases release probability (Pr) via presynaptic Kv1.1-containing potassium channels, reduces NR2B/NR2A ratio through Src kinase, and prunes the dendritic arbor and spines.

Supplementary Table 1 Time constants of NMDA receptor (NMDAR)-mediated EPSCs at MPP-GC synapses. NMDA receptor-mediated EPSCs were fitted with the equation: $EPSC_{NMDAR} = W(e^{-t/\tau 1} - e^{-t/\tau 2})$. τ_{rise} is given by the equation: $\tau_{rise} = \tau_1 \cdot \tau_2 / (\tau_1 - \tau_2)$, and $\tau_{decay} = \tau_1$. The fitting was abandoned if the current was small, where noise greatly affected the fitting accuracy. Two-tailed Student's t test was used to compare immature animals to their mature counterparts. Mature transgenic mice were compared to mature wild-type mice. All numbers are mean ± SEM, with number of cells in parentheses. *, $p < 0.05$

Neuron	NR2A-containing NMDAR		NR2B-containing NMDAR		NR2C/D-containing NMDAR	
	τ_{rise} (ms)	τ_{decay} (ms)	τ_{rise} (ms)	τ_{decay} (ms)	τ_{rise} (ms)	τ_{decay} (ms)
Immature wt	3.76 ± 0.30 (8)	43.8 ± 4.1 (8)	3.53 ± 0.55***** (8)	128.6 ± 24.7***** (8)	14.5 ± 2.4 (8)	418.3 ± 95.2 (7)
Immature mLGI1	3.65 ± 0.30 (9)	43.3 ± 3.7 (9)	2.79 ± 0.73 (9)	108.0 ± 23.8 (6)	19.6 ± 3.7 (9)	412.0 ± 70.5 (9)
Immature LGI1 OE	5.15 ± 0.81 (4)	36.7 ± 4.3 (4)	3.92 ± 1.74 (4)	100.7 ± 32.6 (4)	15.1 ± 4.6 (4)	282.0 ± 41.9 (4)
Mature wt	3.77 ± 0.35 (9)	44.8 ± 2.4 (9)	2.07 ± 0.21 (9)	70.9 ± 12.8 (8)	26.8 ± 5.6 (9)	353.9 ± 38.1 (9)
Mature mLGI1	3.24 ± 0.38 (11)	44.0 ± 2.2 (11)	3.98 ± 0.67***** (11)	68.3 ± 10.9 (11)	28.5 ± 5.4 (11)	399.8 ± 31.0(11)
Mature LGI1 OE	3.36 ± 0.49 (9)	48.0 ± 2.6 (9)	1.52 ± 0.25 (8)	56.9 ± 7.8 (8)	38.0 ± 5.5 (9)	378.9 ± 26.1 (9)

Supplementary Note

Supplementary Figs. 1,2 illustrate the constructs used to produce LGI1 transgenic mice. **Supplementary Fig. 3** indicates that LGI1 mRNA transcription is increased in transverse brain sections in LGI1 transgenic mice probed with a riboprobe against LGI1 exon 1–2 junction. **Supplementary Fig. 4** shows that lateral perforant path (LPP) release probability is not modulated by Kv1 channel blocker α-dendrotoxin (DTX), indicating that developmental decreases of medial perforant path (MPP) release probability do not result from an outgrowth of LPP into the middle molecular layer. **Supplementary Fig. 5** shows different forms of short-term plasticity in LGI1 transgenic mice. High frequency stimulation of MPP fibers (10 Hz, 10 s) produced three types of short-term plasticity of MPP-GC excitatory postsynaptic currents (EPSCs): facilitation (F), depression (D), and augmentation (AUG). As observed for release probability, short-term plasticity of MPP-GC synapses was bi-directionally regulated by mutant LGI1 and excess wild-type LGI1. **Supplementary Fig. 6** shows that Src kinase and phospho-Erk (p-Erk) remain high in mature ATLDE mutant LGI1 mice. **Supplementary Fig. 7** summarizes the developmental change in biophysical properties of dentate granule cells. The biophysical properties and excitability of both immature and mature dentate granule cells are normal in LGI1 transgenic mice. **Supplementary Fig. 8** demonstrates how we extract aberrant EEG segments from raw EEG recordings. **Supplementary Fig. 9** illustrates 4 types of aberrant EEG patterns associated with PTZ kindling experiments. The normalized theta band power is proportional to the severity of aberrant EEG patterns. Based on this observation we unbiasedly characterized over 340 EEG recordings by calculating their normalized theta band power of extracted aberrant EEG segments. **Supplementary Fig. 10** confirms that mice carrying ADLTE mutant LGI1 are more susceptible to PTZ kindling epileptogenesis using behavioral Racine scoring method. **Supplementary Fig. 11** shows that once the mice are kindled by repeated PTZ injections, there are no differences in the latency and duration of clonic seizures across different genotypes. Mice carrying mutant LGI1 exhibited a faster kindling rate (fully kindled state was reach in ~3 injections for mLGI1 compared to ~7 injections for wild-type and LGI1 OE mice; **Supplementary Fig. 9b**). Note there is a decreased latency when clonic seizures are repeatedly triggered by further PTZ injections in kindled mice. Long-lasting late stage tonic-clonic seizures (such as status epilepticus) were rare under our PTZ injection protocol (total 12 injections). **Supplementary Fig. 12** summarizes the major findings of this research. **Supplementary Table 1** summarizes the kinetics of different NR2 subunit-containing NMDA receptor currents.

Supplementary Methods

Slice preparation. Mice were anaesthetised with 2,2,2-tribromoethanol (0.25 mg/g body weight) and transcardially perfused with ice-cold sucrose-containing cutting solutions (in mM: 234 Sucrose, 5 KCl, 1.25 NaH_2PO_4, 5 $MgSO_4$, 26 $NaHCO_3$, 25 Dextrose, 1 $CaCl_2$, balanced with 95% O_2 / 5% CO_2). The brain was then removed after decapitation. The brain areas containing hippocampus were dissected rapidly and transferred to a chamber filled with ice-cold cutting solution. Transverse slices of hippocampus (280 μm) were cut with a tissue slicer (Vibratome 3000 plus) and incubated in oxygenated (95% O_2 / 5% CO_2) artificial cerebrospinal fluid (ACSF, in mM: 125 NaCl, 3 KCl, 1.25 NaH_2PO_4, 1 $MgCl_2$, 26 $NaHCO_3$, 25 Dextrose, 2 $CaCl_2$) at room temperature for at least 1 h before being transferred to the recording chamber at 35–36 °C. Brain slices prepared from adult mice were pre-heated to 35 °C for 30 min before being incubated at room temperature. A cut was made through the hilus to limit the mossy fiber influence.

Electrophysiological recording. Whole-cell recordings of dentate granule cells (GCs) were performed on brain slices of hippocampus. GCs were identified under infrared differential interference contrast (IR-DIC) optics based on their location and morphology and patched with 4–6 MΩ glass pipettes filled with artificial intracellular fluid (in mM: 135 KCH_3SO_3, 4 KCl, 2 NaCl, 10 HEPES, 4 Mg-ATP, 0.3 Tris-GTP, 7 $Tris_2$-Phosphocreatine). Pipettes were connected to the headstage of a Heka EPC 10 amplifier (Heka Elektronik) and fast and slow capacitance and series resistance compensations were carefully adjusted. Liquid junction potentials were not corrected. Series resistance was normally less than 20 MΩ and recordings exceeding 20% change in series resistance were terminated and discarded. Recordings were filtered at 2.9 kHz and digitized at 50 kHz.

Basic biophysical and firing properties were recorded in current-clamp mode using the above KCH_3SO_3-based internal solution and regular ACSF. Input resistance was estimated with a negative square pulse (–25 pA, 200 ms). Membrane time constant was obtained by fitting a single exponential equation to the voltage response to this small negative current pulse. Positive current steps (duration: 0.8 s) were used to acquire the firing property.

Excitatory postsynaptic currents (EPSCs) were recorded at a holding potential of -80 mV (E_{Cl}). An extracellular, glass electrode filled with ACSF was placed at the middle molecular layer 200 μm away from the recording site (medial perforant path, MPP). Presynaptic axons were stimulated using current pulse stimuli (duration = 180 μs，amplitude = 0.5–40 μA, and frequency = 0.1–0.2 Hz for baseline condition) delivered via a constant-current stimulator. Paired-pulse facilitation experiments were carried out to estimate the release probability. The peak amplitude of MPP-GC EPSCs evoked by two identical stimuli separated by 20 ms was measured. The facilitation ratio (the second peak

amplitude/the first peak amplitude) was calculated.

NMDA receptor-mediated EPSCs ($EPSC_{NMDAR}$) were recorded at a holding potential of +40 mV (to remove Mg^{2+} block) in the presence of 10 μM DNQX, 100 μM picrotoxin, and 20 μM glycine. The position of the stimulating electrode and the current pulse stimuli were identical to AMPA receptor-mediated EPSC recording. Cesium-based artificial intracellular fluid (in mM: 100 $CsCH_3SO_3$, 20 KCl, 10 HEPES, 4 Mg-ATP, 0.3 Tris-GTP, 7 $Tris_2$-Phosphocreatine, 3 QX-314) was used to eliminate contamination by K^+ and Na^+ currents. Ro 25-6981 (0.5 μM, NR2B-specific blocker), PPDA (5 μM, potent NR2C/2D blocker), and APV (100 μM) were used to separate receptor subtypes of the $EPSC_{NMDAR}$.

To record spontaneous synaptic currents, a low divalent ion ACSF (in mM: 125 NaCl, 3.5 KCl, 1.25 NaH_2PO_4, 0.5 $MgCl_2$, 26 $NaHCO_3$, 25 Dextrose, 1 $CaCl_2$) was used. Using pipettes filled with cesium-based internal fluid (see above), spontaneous EPSCs (sEPSCs) were recorded at a holding potential of –60 mV and spontaneous IPSCs (sIPSCs) were recorded at a holding potential of +10 mV. Miniature EPSCs (mEPSCs) were recorded at –60 mV using cesium-based internal fluid and regular ACSF containing 0.5 μM TTX and 50 μM picrotoxin. Miniature IPSCs were recorded at +10 mV using cesium-based internal fluid and regular ACSF containing 0.5 μM TTX, 10 μM DNQX, and 50 μM APV. Continuous data were recorded in 10 sec sweeps, filtered at 1 kHz and sampled at 20 kHz. Individual events were counted and analyzed with MiniAnalysis software (Synaptosoft). 300 s of mini events randomly chosen from 5 cells in each genotype are analyzed. The amplitude histograms were binned at 1 pA. Differences between cumulative amplitude histograms were evaluated by the Kolmogorov-Smirnov test.

Field excitatory synaptic potential (fEPSP) was elicited by stimulating the MPP and recording with a regular ACSF-filled patch pipette placed in the GC layer 200 μm from the stimulating electrode. Traces were averaged 20 times to eliminate noises. Since afterdischarges were not present in all traces being averaged and their latencies were not fixed, averaging weakened the afterdischarge signals. To characterize afterdischarges, individual noisy traces were down-sampled at 250 Hz and filtered with a finite impulse response (FIR) filter. The amplitude of population spikes recorded in picrotoxin was normalized to baseline population spike amplitude. Maximum baseline population spike amplitude was not significantly altered by genotype (WT, 0.95 ± 0.12 mV, $n = 7$; mLGI1, 0.64 ± 0.19 mV, $n = 5$; LGI1 OE, 1.11 ± 0.50 mV, $n = 5$; wt vs. mLGI1, $P = 0.22$; wt vs. LGI1 OE, $P = 0.76$).

Histochemistry. Intracellular solution containing 0.5% biocytin was used to fill GCs. Brain slices of hippocampus with biocytin-filled GCs were fixed in 4% para-formaldehyde in PBS for 24 h. After fixation, hippocampal slices were washed with PBS and then exposed to blocking solution (1% H_2O_2 and 10% methanol in PBS) for 30 min to block endogenous peroxidases. After being washed in PBS, hippocampal slices

were incubated in avidin-biotinylated horseradish peroxidase (ABC-Elite kit, Invitrogen) mixed with Triton X PBS (0.75% Triton X in PBS) for 2–4 h. After peroxidase incubation, slices were washed with PBS and then incubated in predeveloping solution (0.02% DAB in PBS) for 30 min. Slices were immediately transferred to slides and several drops of developing solution (0.02% DAB and 0.03% H_2O_2 in PBS) were added. Stained cells should be visible under the microscope within 5 min. After developing, slices were immediately washed in PBS. Developed slices were mounted with Mowiol (4.8% Mowiol 4-88, 12% glycerol, 0.2 M tris). Detailed morphology of GCs was reconstructed using a Nikon microscope equipped with an ApoPlan 100x/1.4 oil immersion objective under the control of Neurolucida software (MicroBrightField).

***In-situ* hybridization**. Brain tissues from 4–8 weeks old mice were fixed in ice-cold 4% paraformaldehyde solution for 4–6 h. After the brain tissues were rinsed and penetrated with ice-cold 30% sucrose in PBS, 20 μm transverse sections were cut from frozen brain tissues embedded in optimal cutting temperature compound (OCT). LGI1 expression was detected by using digoxigenin-labeled riboprobes against LGI1 exon 1–2 junction as previously reported[11]. Sections were mounted and hybridized with the probes overnight. Sections were then incubated with alkaline phosphatase-conjugated anti-digoxigenin antibody and developed in nitro blue tetrazolium and 5-bromo-4-chloro-3-indolyl phosphate containing solutions for 24 h. LGI1 mRNA distribution was examined under a Zeiss Axioplan2 microscope and images were captured with Axiovision 4.5 software (Zeiss). Custom Matlab (Mathworks) script was written for analyzing the optical densities of *in situ* images. The optical densities of stained cells in dentate gyrus and entorhinal cortex were corrected for uneven background densities.

Western blot. Mouse brain samples were obtained and homogenized using a chilled Tenbroeck tissue homogenizer containing 2 ml of chilled STE buffer (in mM: 320 Sucrose, 20 Tris, 2 EDTA, 200 μg/ml PMSF, pH 8.0) with protease and phosphatase inhibitors (1 μg/ml leupeptin, 1 mg/ml pepstatin, 1 μg/ml aprotinin, 1 mM NaF, 1 mM Na_3VO_4). The homogenate was then centrifuged at 14,000 g for 1 h at 4 ^oC and the supernatant removed. The pellet was resuspended in chilled TET buffer (in mM: 20 Tris, 1 EDTA, 1.3% Triton X-100, pH 8.0) with protease and phosphatase inhibitors and centrifuged at 100,000 g for 1 h. 10% SDS-PAGE was used to separate protein samples. After electrophoresis, the gels were transferred to nitrocellulose membranes using a constant voltage of 70–80 V for 90 min. The membranes were then blocked in 5% milk in TTBS (50 mM Tris-HCl, pH 8, 150 mM NaCl, 0.05% Tween 20) for one half hour at room temperature on a rocker and incubated in the primary antibody overnight on a rocker at 4 ^oC. Primary antibodies were made with 5% milk in TTBS solutions (LGI1, 1:250, Santa Cruz; β-actin, 1:250, Cell Signalling; Src, 1:1,000, Cell Signalling; ADAM22, 1:1,000, NeuroMab; PSD95, 1:1,000, NeuroMab). Following primary antibody incubation, the membranes were rinsed three times in TTBS before being

incubated with horseradish peroxidase-conjugated secondary antibody (1:10,000 in 5% milk in TTBS) for 1 h on a rocker at room temperature. After being washed in TTBS four times on a rocker at room temperature, the membranes were then developed using either ECL or ECL-Plus Western blotting detection reagents.

PTZ kindling. Mice, at 6–8 weeks of age, received intraperitoneal injections of PTZ (30 mg/kg) every other day for 12 consecutive injections. The behavioural consequences of PTZ were monitored for 30 min following each injection. The severity of convulsive responses was classified according to the Racine score: 0, no response; 1, mouse and facial jerks; 2, nodding or myoclonic body jerks; 3, forelimb clonus; 4, loss of posture, hindlimb clonus and forelimb tonus; 5, hindlimb tonus, status epilepticus and/or death.